PERGAMON

Microelectronics Reliability 40 (2000) 919–932

MICROELECTRONICS RELIABILITY

www.elsevier.com/locate/microrel

Introductory invited paper

Mechanisms of noise sources in microelectromechanical systems

Zoran Djurić *

IHTM – Institute of Microelectronic Technologies and Single Crystals, Njegoševa 12, 11000 Belgrade, Yugoslavia

Received 25 November 1999

Abstract

It is well known that several mechanisms of noise generation appear in microelectronic devices, causing thermal noise, shot noise, generation–recombination noise and $1/f$ noise. Besides these noises, in the case of microelectromechanical systems, specific additional noises appear as a consequence of the fact that the "building blocks" (microcantilevers or membranes) of micromechanical systems have very small geometrical dimensions and mass. Most often, these noises are the consequences of temperature fluctuations caused by dissipative processes in various vibrational structures within the micromechanical systems. This work presents a methodology of calculation of noises, characteristic of microelectromechanical systems and applies it to the calculation of limiting performances of accelerometers, sensing probe cantilevers and thermal infrared detectors.

1. Introduction

The development of microsystem technologies (surface and bulk micromachining) resulted in the fabrication of miniature sensors, electromechanical parts and actuators [1]. Their coupling into a single chip with integrated circuits furnished the so-called microelectromechanical systems (MEMS). These miniature systems can in principle replace completely the existing measuring instruments, for instance spectrophotometers, ellipsometers, etc.

In the current development stage, there is an independent interest for miniature sensor and actuator parts for microsystems, and very recently, a great demand arose for miniature microelectromechanical filters, resonator circuits, etc. which could replace quartz resonators and filters with surface acoustical waves. This replacement would result in a complete miniaturization of wireless communication instruments [2].

It is interesting to note that all the above-microelectromechanical parts consist of only a relatively small number of different "building blocks". These are primarily various kinds of cantilevers and diaphragms. Their geometry may vary, and they can be made of various materials – metals, semiconductors and dielectrics. Depending on their function, they can be multilayered. Such is the case with bimaterial cantilevers and with diaphragms serving at the same time as optical filters, etc.

Characteristic for all these building blocks are their miniscule dimensions. Consider an example, the cantilever for a highly sensitive SPM microscope. According to Ref. [3], to achieve a force resolution of 5.6×10^{-18} $N/Hz^{1/2}$ at 4.8 K in vacuum, a single-crystal silicon cantilever was only about 600 Å thick, 100 μm long and 10 μm wide. The weight of this cantilever was of the order of about 10^{-13} kg.

A similar situation is encountered in micromechanical resonators [4], where a resonant frequency in gigahertz range is required. For instance, the approximate dimensions of a clamped–clamped beam resonator required to reach a frequency of 1 GHz are a length of 4 μm, a width of 2 μm and a thickness of 2 μm. The weight of this cantilever is only 3.5×10^{-14} kg.

For the author of this work, who has been working for a long time in the field of infrared detectors, it is interesting that to achieve a high detectivity and fast response in a thermal detector, it is necessary to have

* Tel.: +381-11-638-188; fax: +381-11-182-995.
E-mail address: zdjuric@chem.bg.ac.yu (Z. Djurić).

0026-2714/00/$ - see front matter
PII: S0026-2714(00)00004-4

a large heat resistance between the sensing element (membrane) and the ambient (radiative resistance-limited case), whereas the heat capacity (proportional to the mass of the absorptive area) should be the smallest possible [5]. On the contrary, it is well known that the detectivity in real situations increases with the active area. A compromising solution is to couple the active area with its surroundings by small cross-section, thermally isolating beams and to keep the thickness of the sensitive membrane small.

This work is dedicated to the determination of the limiting performance of the microsystems utilizing the above "building blocks". For example, the performance of a sensor is improved by reducing noises in the preamplifier used to convert physical signals into electric ones and by the control over other error sources like for example non-compensated thermal drift. If this is done, a point is achieved where the processes causing thermodynamical fluctuations start posing the barrier for any further improvement of sensor parameters [6–8].

In the first approximation, all of these structures can be modeled as a damped mechanical oscillator. The damping is connected with the fact that the cantilever is surrounded by a medium with a given viscosity which resists its movement. Besides this, the damping can be caused by internal processes on the surface and in the bulk of the cantilever [9].

This is especially marked if the external viscous effects are eliminated by placing the cantilever in vacuum. The dissipative processes in this case are very similar to the dissipative processes in gravitational antennas [10,11]. They start to depend on the way the cantilevers are fastened, on their surface treatment, etc. Of special interest are the effects caused by the fact that the weight of such elements is very small. The absorption–resorption effects cause the fluctuations of the resonant frequency even in a 10^{-4} Torr vacuum by changing the resonator mass [12,13].

In any case, if the temperature of a damped mechanical resonator is finite and if the system is in thermodynamical equilibrium, the mechanical resonator must show a certain degree of random movement by which the environment returns the resonator energy lost by damping. These random vibrations are the cause of the thermal–mechanical noise.

It stems from the preceding text that each dissipative mechanism is connected with a corresponding noise, which is actually the basic meaning of the fluctuation–dissipation theorem.

In certain situations, temperature fluctuations can be caused by random variations of the number of photons arriving from the background and being absorbed or being emitted from the sensitive element. If the temperatures of the detector and its environment are different, they cannot be calculated utilizing the fluctuation–dissipation theorem. In this article, they are calculated by utilizing a kind of generation–recombination processes.

2. Theory of mechanical–thermal noise

Macroscopic motion of a body surrounded by an external medium is followed by irreversible friction processes, which eventually cause the motion to stop. The kinetic energy of the body is transformed into heat or dissipated. A purely mechanical consideration of this motion is not possible in a general case.

However, there are important practical situations where the state of the system in a given moment can be fully described by its coordinate Q_i and the speed (velocity) $\dot{Q}_i$. The described situation applies for the case of small oscillations around an equilibrium position, and corresponds to linear dissipative systems.

The equations of motion which take the dissipation into account can be obtained by introducing additional terms proportional to the velocity into the standard form of the equation for the derivative of the generalized impulse [14,15]:

$$F = \dot{P}_i = -\frac{\partial U(Q_i)}{\partial Q_i} - \sum_{k=1}^{s} \gamma_{ik}\dot{Q}_k, \tag{1}$$

where $U(Q_i)$ is the potential energy of the system. According to the Onsager's principle of symmetry $\gamma_{ik} = \gamma_{ki}$. Thus, the existence of the dissipation processes in the above approximation causes the appearance of additional friction forces, which are linearly dependent on the velocity of motion. These forces can be obtained as the derivative of the function

$$f = \frac{1}{2}\sum_{i,k} \gamma_{ik}\dot{Q}_i\dot{Q}_k, \tag{2}$$

which is called the dissipative function.

The simplest model that can serve as the mentioned dissipative system is a damped mechanical oscillator with mass m, the spring constant κ and the mechanical resistance R. According to Eq. (1), its equation of motion is

$$m\frac{\mathrm{d}^2x}{\mathrm{d}t^2} + R\frac{\mathrm{d}x}{\mathrm{d}t} + \kappa x = F(t), \tag{3}$$

where $F(t)$ represents an external force. The above equation can be written in the form

$$m\frac{\mathrm{d}v}{\mathrm{d}t} + Rv + \kappa\int v\,\mathrm{d}t = F, \tag{4}$$

where $v = \dot{x}$ is the velocity.

The above expression is fully analogous to the equation of the current in an electrical circuit consisting of an inductance L, capacitance C and a resistance R

$$L\frac{\mathrm{d}i}{\mathrm{d}t} + Ri + \frac{1}{C}\int i\,\mathrm{d}t = U(t). \tag{5}$$

By comparing Eqs. (4) and (5), we see that there is the following analogy:

voltage	U	force	F
current	I	velocity	v
inductance	L	mass	m
capacitance	C	(stiffness constant)$^{-1}$	$1/k$
resistance	R_e	mechanical resistance	R

The dissipation mechanisms are connected with the friction forces opposing the motion of the body within a medium. They depend on the velocity, shape and dimensions of the body and on the properties of the medium. Besides the above friction forces, in the case of real bodies, there is also "internal" damping.

In order to include internal damping in a material, the basic model of a simple harmonic oscillator described by

$$m\ddot{x} + \kappa x = F \tag{6}$$

must be modified [10,16] to include dissipation. A general way to take dissipation into account is to introduce a small imaginary part into the spring constant

$$\kappa \to \kappa(1 + \mathrm{i}\Phi). \tag{7}$$

If the force F is sinusoidal, the response x of the spring will lag the force by the angle $\Phi(\omega)$. In this case, Eq. (6) becomes

$$-m\omega^2 x + \kappa(1 + \mathrm{i}\Phi(\omega))x = F. \tag{8}$$

This new equation of motion takes into account the dissipation because it includes a component of the restoring force which is out of phase with the displacement.

If the ambient temperature around the damped mechanical oscillator is finite (i.e., not 0 K) and if the system is in thermal equilibrium, then the mechanical oscillator must exhibit some degree of random motion. These random vibrations constitute the thermal–mechanical noise.

The magnitude of the random vibrations is dependent on the extent of damping in the oscillator. This is connected with the fact that to avoid violating the Second Law of Thermodynamics, the model of a damped harmonic oscillator must include a noise force generator with a sufficient amplitude to maintain the degree of random vibration dictated by the temperature of the system. Without this noise force generator, the damping of the system would stop any oscillation, implying a system temperature of 0 K, which would violate the condition of the thermal equilibrium at any temperature different from 0 K.

On the contrary, a thermodynamical system in equilibrium is characterized by two classes of parameters: the "extensive" parameters like the volume or the number of moles, and the "intensive" ones or the "generalized forces" (e.g. pressure or chemical potential). The values of these parameters cannot be accurately determined due to random vibrations or the existence of spontaneous fluctuations.

The fluctuations of the appropriate generalized "force" are related not to the standard thermodynamic parameters of the system, but to the extent of damping. An equation for the voltage fluctuation (a "generalized force") in a linear electrical system was derived by Nyquist in 1928. The Nyquist equation is unique in physics, correlating a property of a system in equilibrium (voltage fluctuation) with a parameter characterizing an irreversible damping process (i.e. electrical resistance). The equation not only gives the mean square fluctuation voltage, but also provides the frequency spectrum of the fluctuations.

The extension of the Nyquist theorem to a general linear dissipative system was presented by Callen and Welton in 1951 [17]. This general theorem determines the connection between the "impedance" of a general linear dissipative system and the fluctuations of a generalized "force".

Using the quantum theory of time-dependent perturbations, Callen and Welton obtained the following mathematical form of the fluctuation–dissipation theorem:

$$\langle F^2\rangle = \frac{2}{\pi}\int R(\omega)E(\omega,T)\,\mathrm{d}\omega, \tag{9}$$

where

$$E(\omega,T) = \frac{1}{2}\hbar\omega + \frac{\hbar\omega}{\exp\frac{\hbar\omega}{kT} - 1}, \tag{10}$$

and $R(\omega)$ is the real part of the impedance Z defined as

$$F = Z(\omega)\dot{Q}, \tag{11}$$

where all quantities are now assumed to be written in the standard complex notation.

As can be seen, $E(\omega,T)$ is formally the expression for the mean energy of an oscillator with a frequency ω and at a temperature T. At higher temperatures ($kT \gg \hbar\omega$, $E(\omega,T) \approx kT$), the spectral distribution of the thermal driving force is given by

$$F_{\mathrm{th}}^2(\omega) = \frac{\mathrm{d}\langle F^2\rangle}{\mathrm{d}f} = 4kT\,R(\omega), \tag{12}$$

where, for the case described by Eq. (8), $R(\omega)$ is the mechanical resistance, the real part of the impedance $Z = F/v$. Equivalently, the expression for the displacement power spectrum

$$X^2(\omega) = \frac{4kT}{\omega^2}\,\mathrm{Re}\,Y(\omega). \tag{13}$$

$\mathrm{Re}\,Y(\omega)$ is the real part of the admittance $Y(\omega) = Z^{-1}(\omega)$.

From Eq. (8), we obtain the mechanical impedance for the simple harmonic oscillator with damping as

$$Z = \frac{F}{v} = \frac{F}{\mathrm{i}\omega x} = \frac{-m\omega^2 + \kappa(1 + \mathrm{i}\Phi(\omega))}{\mathrm{i}\omega}$$
$$= \mathrm{i}m\omega + \frac{\kappa}{\mathrm{i}\omega} + \frac{\kappa\Phi(\omega)}{\omega}. \tag{14}$$

The admittance is

$$Y = \frac{\omega\kappa\Phi + \mathrm{i}(\omega\kappa - m\omega^3)}{(\kappa - m\omega^2) + \kappa^2\Phi^2}. \tag{15}$$

According to Eq. (13), the spectral density of thermal noise power is given by

$$S_x(\omega) = X^2(\omega)$$
$$= \frac{4kT}{m\omega_0^2}\,\frac{\Phi(\omega)}{\omega}\,\frac{1}{\left[1 - (\omega/\omega_0)^2\right]^2 + \Phi^2(\omega)} \tag{16}$$

with $\omega_0^2 = \kappa/m$.

The integral of $\chi^2(\omega)$ over all frequencies corresponds to the energy per one degree of freedom $kT/2$, as one could expect from the equipartition theorem.

Various models of thermal noise almost invariably assume that the dissipative force is proportional to the velocity. If we compare Eq. (3) in a complex form to Eq. (8), we obtain

$$R\omega = \kappa\Phi(\omega), \tag{17}$$

and Eq. (16) assumes its usual form [7,8]

$$X(\omega) = \sqrt{4\kappa T/(\omega_0 Q\kappa)}\,G(\omega), \tag{18}$$

where

$$G(\omega) = \left(\left(1 - (\omega/\omega_0)^2\right)^2 + (\omega/\omega_0)^2/Q^2\right)^{-1/2}, \tag{19}$$

while the Q-factor of the mechanical oscillatory circuit is

$$Q = \omega_0 m/R = 1/\Phi(\omega_0). \tag{20}$$

However, in low-loss oscillators, the dependence of the dissipation on frequency seldom obeys this behavior. In order to model a large variety of loss mechanisms, $\Phi(\omega)$ is allowed to become an arbitrary function of ω. For example, in the description of materials, the elastic losses are characterized by adding an imaginary part to Young's modulus: $E = E_0(1 + \mathrm{i}\Phi)$. In this case, the parameter Φ is referred to as the material's "internal friction" or loss function. Generally, E_0 and Φ are frequency-dependent. For example, viscous friction in a material would be described by a function Φ linearly dependent on frequency. $\Phi(\omega)$ and $E_0(\omega)$ are not completely independent, as they are related by the Krammers–Kronig relations. Of course, this relation is also valid for κ and Φ:

$$\kappa(\omega) - 1 = \frac{2}{\pi}\int_0^\infty \frac{x\Phi(x)}{x^2 - \omega^2}\,\mathrm{d}x,$$
$$\Phi(\omega) = -\frac{2\omega}{\pi}\int_0^\infty \frac{\kappa(x)}{x^2 - \omega^2}\,\mathrm{d}x. \tag{21}$$

But as long as $\Phi \ll 1$, the frequency dependence $E_0(\omega)$ remains very weak, and the transition described by Eq. (7) is justified.

It is sometimes necessary to take account of the fact that real oscillators are distributed systems, and the description with point masses and massless springs is not justified [18]. For example, a real microcantilever exhibits transverse vibrational modes, as well as longitudinal modes of its mass. This means that Eq. (16) or Eq. (18) applied to the fundamental mode of the cantilever will cease to apply at a high enough frequency, as eventually the thermal noise from another mode at a higher resonant frequency will dominate. This means that better estimates of the thermal noise effects on the cantilever displacement and the error involved in using a single mode approximation (or a single spring mass-damper system) can be obtained using a multi-mode model.

The linearized equation of motion describing the transverse deflection $y(x,t)$ of a beam as a function of the longitudinal coordinate x and time t can be expressed as [19]:

$$EI\frac{\partial^4 y}{\partial x^4} - p\frac{\partial^2 y}{\partial x^2} + C\frac{\partial y}{\partial t} + \rho S\frac{\partial^2 y}{\partial t^2} = f(x,t), \tag{22}$$

where ρ denotes the specific mass, S is the cross-section area of the beam, C is the viscous drag parameter (drag force per unit length and unit velocity), $f(x,t)$ denotes a transverse force per unit length and represents all externally applied mechanical forces, E is Young's modulus of the beam material, and I is the second moment inertia (For a beam width with rectangular cross-section $I = bh^3/12$, b and h are the width and the thickness of the beam, respectively) at the beam cross-section, p is the applied axial force. Eq. (22) applies for a beam in which $b \approx h$. For the so-called wide beams, i.e. $b > 5h$, Young's modulus is effectively replaced by $E/(1 - \nu^2)$, where ν denotes Poisson's ratio.

Using the modal analysis techniques [20], the solution of Eq. (22) can be written as follows:

$$y(x,t) = \sum_{n=1}^{\infty}\psi_n(x)q_n(t), \tag{23}$$

where $\psi_n(x)$ are the normalized mode shapes and $q_n(t)$ are generalized coordinates. Introducing Eq. (23) into the equation of motion (22) and multiplying each term

by a normal mode $\psi_m(x)$, integrating along the beam length and utilizing the orthogonality of the mode shapes

$$\frac{1}{l}\int_0^l \psi_n(x)\psi_m(x)\,\mathrm{d}x = \delta_{nm} \tag{24}$$

leads to

$$M_n\ddot{q}(t) + r_n\dot{q}(t) + \kappa_n q(t) = F_n(t) = F_n e^{i\omega t}, \quad n = 1,2,\ldots, \tag{25}$$

where

$$M_n = \int_0^l \rho S\psi_n^2(x)\,\mathrm{d}x = \rho S l = m \tag{26}$$

is the generalized mass corresponding to the mode n,

$$\kappa_n = \int_0^l \psi_n(x)\left(EI\frac{\partial^4\psi_m(x)}{\partial x^4} - p\frac{\partial^2\psi_m(x)}{\partial x^2}\right)\mathrm{d}x = \omega_n^2 M_n \tag{27}$$

is the generalized stiffness corresponding to the mode n and

$$r_n = \int_0^l C\psi_n^2(x)\,\mathrm{d}x = Cl \tag{28}$$

is the generalized mechanical resistance corresponding to the mode n.

If we put $f(x,t) = f(x)F_n(t)$, we obtain

$$F_n = \int_0^l f(x)\psi_n(x)\,\mathrm{d}x, \tag{29}$$

the generalized load corresponding to $f(x)$ and the mode n.

Eq. (25) represents an infinite set of uncoupled ordinary differential equations for a simple clamped mechanical oscillator.

The mode shapes $\psi_n(x)$ are determined using a special eigenvalue problem formulated as

$$L[\psi(x)] = \omega^2 m\psi(x), \tag{30}$$

where $L = EI(\partial^4\psi/\partial x^4)$.

The eigenvalue problem consists of seeking the values of the parameter ω^2 for which there is a non-vanishing function ψ satisfying the preceding differential equation and the appropriate boundary conditions. Each eigenvalue (in our case ω_n) and the corresponding eigenfunction ($\psi_n(x)$) define a mode of the system. The problem is homogeneous so that the amplitudes of the eigenfunctions are arbitrary and only the shapes of the eigenfunctions can be uniquely determined.

For instance, the eigenfunctions of a cantilever (clamped-free) beam of a length l are found to be

$$\psi_{n\mathrm{CF}}(x) = \cos(k_n x) - \cosh(k_n x) - \frac{\cos(k_n l) + \cosh(k_n l)}{\sin(k_n l) + \sinh(k_n l)} \times (\sin(k_n x) - \sinh(k_n x)) \tag{31}$$

and for a clamped–clamped beam

$$\psi_{n\mathrm{CC}}(x) = \cos(k_n x) - \cosh(k_n x) + \frac{\cos(k_n l) - \cosh(k_n l)}{\sin(k_n l) - \sinh(k_n l)} \times (\sin(k_n x) - \sinh(k_n x)), \tag{32}$$

where k_n is a constant corresponding to the mode n.

It is easily verified that

$$\frac{1}{l}\int_0^l \psi_n(x)\psi_m(x)\,\mathrm{d}x = \delta_{nm}. \tag{33}$$

The corresponding natural frequencies are connected to the constants k_n as

$$\omega_n^2 = k_n^4(EI/\rho S). \tag{34}$$

The constants k_n are determined from the characteristic equation, which is a direct result of solving the special eigenvalue problem and taking into account the appropriate boundary conditions.

For the clamped–clamped beam, the characteristic equation is given as

$$\cos(kl)\cosh(kl) = 1, \tag{35}$$

yielding, for the fundamental mode, $k_1 l \approx 4.730$ and for the cantilever

$$\cos(kl)\cosh(kl) = -1 \tag{36}$$

yielding $k_1 l = 1.875$ (Fig. 1).

As an example, consider a situation when a force $f(x,t)$ is applied at the end of the system $x = L$. In order to obtain an equation similar to Eq. (3), for the mode n, it is necessary to multiply Eq. (25) with $\psi_n(L)$. We obtain

$$m\ddot{y}_n(L,t) + r\dot{y}_n(L,t) + M\omega_n^2 y_n^2 = F\psi_n^2(L)e^{i\omega t}, \tag{37}$$

or in Saulson's notation [10]

$$m\ddot{y} + \kappa y = F\psi_n^2(L)e^{i\omega t}. \tag{38}$$

If we replace $\kappa_n = \kappa_n(1 + i\Phi_n(\omega))$ in Eq. (38), we obtain the complex form

$$\{-\omega^2 M + \omega_n^2 + i\omega_n^2 M\Phi_n(\omega)\}y_n = F\psi_n^2(L), \tag{39}$$

$$y_n = \frac{F\psi_n^2(L)}{M(\omega_n^2 - \omega^2 + i\omega_n^2\Phi_n(\omega))}. \tag{40}$$

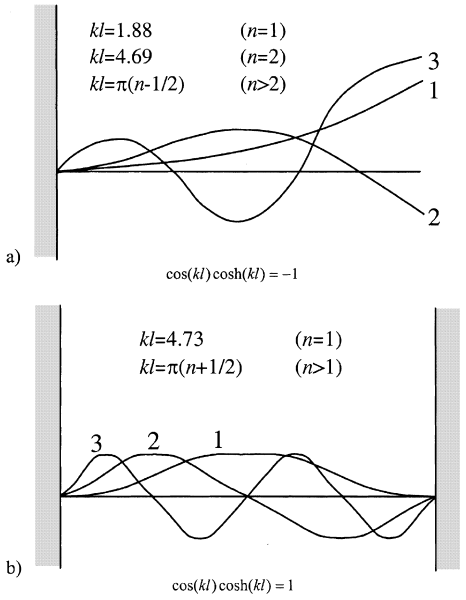

Fig. 1. Fundamental modes for (a) the cantilever and (b) the clamped–clamped beam.

Thus, the admittance $Y = v/F = \mathrm{i}\omega y/F$ is given as

$$Y_n = \frac{\mathrm{i}\omega\psi_n^2(L)}{M(\omega_n^2 - \omega^2 + \mathrm{i}\omega_n^2\Phi_n(\omega))}. \tag{41}$$

From the fluctuation–dissipation theorem and Eq. (18), we can now find the thermal noise displacement at $x = L$ from

$$y^2(\omega) = \frac{4kT}{M\omega}\sum_{n=1}^{\infty}\frac{\psi_n^2(L)\Phi_n(\omega)}{\omega_n^2\left[\left(1-(\omega/\omega_n)^2\right)^2 + \Phi_n^2(\omega)\right]}. \tag{42}$$

3. Dissipative mechanisms

In a narrower sense, the dissipative mechanisms determining the mechanical–thermal noise are connected with the friction forces opposing the body motion. As mentioned in Section 1, these processes can be divided into two groups: external velocity damping and internal damping.

External velocity damping is connected with the friction forces opposing the motion of the body within the surrounding medium. It depends on the velocity, shape and dimensions of the body and on the properties of the medium. For small values of the Reynold's number ($\mathrm{Re} < 2000$)

$$\mathrm{Re} = \rho v L/\mu, \tag{43}$$

where ρ is the fluid density, v, the velocity, L, the characteristic dimension and μ is the viscosity, we can assume that the friction force is linearly proportional to the velocity. With an increase of the velocity, the friction force dependence on velocity changes.

For low velocities, the friction force is

$$F_r = Rv, \tag{44}$$

where the coefficient of mechanical resistance is frequency (ω)-independent. In the approach utilizing the loss function $\Phi(\omega)$

$$R = \kappa\Phi(\omega)/\omega \tag{45}$$

to have a frequency-independent R, the function $\Phi(\omega)$ should be proportional to ω.

In the case of capacitive pressure sensors, acoustic sensors or micromechanical oscillators, the interelectrode distance is of an order of a few micrometers or lesser, because of the requirement for the minimum possible applied voltage. This causes the squeeze-film damping, i.e. the viscous losses caused by the squeezing out of the fluid between the moving parts [7]. For two parallel discs with equal surfaces S at a mean distance h_0, the equivalent mechanical resistance is

$$R_{\mathrm{film}} = \frac{3\mu S^2}{2\pi h_0^3}, \tag{46}$$

where μ is the fluid viscosity (1.8×10^{-5} kg/ms for the air at 20°C, 1.0×10^{-3} kg/ms for water at 20°C). To decrease this resistivity, the bottom plate is perforated, so that the fluid flows out through these openings as well. The mechanical resistivity for this case can be approximated as [7]

$$R_{\mathrm{perf}} = \frac{12\mu}{N\pi h_0^2}G(A)S^2, \tag{47}$$

where N is the total number of holes in the perforated plate, A is the plate area with openings and

$$G(A) = \frac{A}{2} - \frac{A^2}{8} - \frac{\ln A}{4} - \frac{3}{8}. \tag{48}$$

The total resistance is obtained by calculating the parallel connection of the R_{film} and R_{perf}.

As the viscosity of gases is pressure dependent, it can be significantly decreased by lowering the pressure. However, at very low pressures or in the case of ultra-thin films, the gas rarefaction effect [21] and the molecular interaction with surfaces effectively change the viscosity.

This effect is taken into account by introducing the effective viscosity μ_{eff}, so that expressions (46) and (47) are still valid for $\mu = \mu_{\mathrm{eff}}$. For the situation presented in Fig. 2, the effective viscosity is a function of the Knudsen number K_n, the ratio between the gas mean free path λ and the air gap height h_0.

The effective viscosity can be expressed as a function of the Knudsen number and the Poisseuille flow-rate coefficient $Q_p(K_n, \alpha_0, \alpha_1)$ as follows:

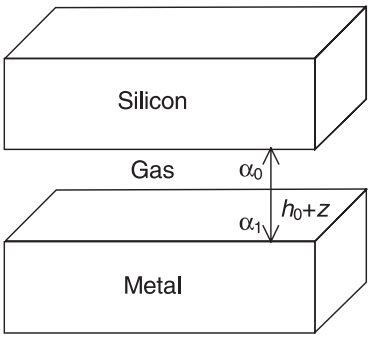

Fig. 2. Schematic of the air gap between the silicon (membrane) and the fixed metallized electrode. The air gap height h_0 is much smaller than the other dimensions. z is a small variation in the plate separation, α_0 and α_1 are the accommodation coefficients.

$$\mu_{\text{eff}} = \frac{\sqrt{\pi}}{12K_nQ_{\text{p}}(K_n,\alpha_0,\alpha_1)}\mu, \tag{49}$$

where α_0 and α_1 are the accommodation coefficients at the boundary surfaces. These coefficients are connected with the surface reflection of the rarefied gas molecules and for example for the specular molecular reflection $\alpha = 0$, whereas for diffuse $\alpha = 1$.

The approximate expression for the flow-rate coefficient for a practical situation (metal–silicon boundary) is

$$Q_{\text{p}}(K_n,\alpha_0,\alpha_1) = \frac{D}{6} + \frac{2-\alpha_0}{\sqrt{\pi}}\ln\left(\frac{1}{D}+2.18\right) + \frac{\alpha_0}{0.642} + \frac{(1-\alpha_0)(D+2.395)}{2+1.12\alpha_0 D} - \frac{1.26+10\alpha_0 D}{1+10.98D} + \frac{\exp(-D/5)}{8.77}. \tag{50}$$

The relative error of this approximate equation is less than $\pm 1\%$ for all values of $D = \pi^{1/2}/2K_n$ and $0 \leqslant \alpha_0 \leqslant 1$.

The dependence of the effective viscosity coefficient μ_{eff} on pressure stems from the dependence of the free path length on pressure p:

$$\lambda = \frac{kT}{\sqrt{2}\pi\sigma^2 p}, \tag{51}$$

where σ is the effective radius of cross-section; for air, it is $\sigma = 3.74 \times 10^{-8}$ cm. Thus, we obtain at room temperature

$$\lambda_{\text{Air}} = \frac{6.68 \times 10^{-3}}{p(\text{Pa})}\,(\text{m}). \tag{52}$$

Fig. 3 shows the dependence of the normalized viscosity on pressure p for different values of the parameter h_0. As the mechanical resistance, according to Eq. (46), is proportional to the effective viscosity, we can see that the evacuation of the medium around the vibrating "building blocks" is an efficient way to decrease the mechanical resistance and thus to increase the Q factor.

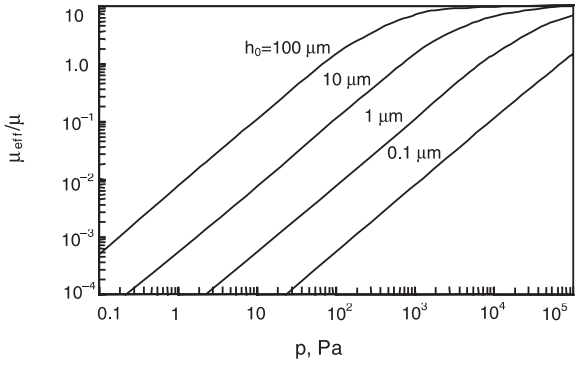

Fig. 3. Dependence of the normalized viscosity on the pressure p for different values of the parameter h_0.

The other main energy loss is caused by internal damping. It is dependent on the material used for a resonator and is influenced by bulk and surface properties as for example dislocations, point defects or impurities.

In the above-mentioned damping, it is necessary to include thermoelastic losses and Akheiser losses. The thermoelastic internal friction is caused by the irreversible heat conduction from the regions of compression to the regions of expansion which occurs during transversal and longitudinal vibrations. The details of these loss mechanisms can be found in Ref. [15].

Akheiser damping occurs because thermally elastic standing-wave pattern at resonance disturbs the equilibrium distribution of thermally excited elastic waves (phonons).

As mentioned in Section 1, if the influence of the viscous effects is entirely suppressed, the mechanical resistance and the loss function $\Phi(\omega)$, and thus the Q factor which is equal to $1/\Phi(\omega_0)$ – are determined by the internal damping.

The experimental and theoretical investigation of the internal damping is intensively performed for gravitational wave interferometers, for which it is required to be capable of detecting broadband gravitational bursts with a strain amplitude sensitivity near 10^{-21} or smaller at frequencies near around 100 Hz [16]. It is clear that the measuring system must be in high vacuum and at a low temperature (4 K).

The investigations performed until now [10,11] showed that the most common functional form for $\Phi(\omega)$ in materials of many kinds is Φ approximately constant over a large band of frequencies. Regardless of the simplicity of this dependence, in this moment, no simple model exists to furnish a general explanation of this phenomenon.

The investigation of the "internal damping" in microsystems is in its infancy. It is surely interesting to try and apply certain results obtained in the field of

gravitational wave detectors to the field of microsystems. In our ensuing consideration of a specific microsystem, we will have an opportunity to see the importance of this kind of damping.

Besides the previously considered "mechanical" dissipation systems, it is especially interesting for us to analyze the dissipation mechanism in thermal detectors [8]. A thermal detector is a sensor which converts incident radiation into electrical signal by a change of its temperature.

To achieve a high sensitivity, the sensitive area of a thermal detector must be thermally well isolated from its surroundings. The equation of heat transfer determining the temperature increase of the sensitive element caused by optical signal power Φ is given as [15]

$$C_{\text{th}}\frac{\mathrm{d}\Delta T}{\mathrm{d}t}+G_{\text{th}}\Delta T=\varepsilon_1\Phi, \tag{53}$$

where ε_1 is the emissivity of the detector active area, G_{th} is thermal conductance and C_{th} is thermal capacitance. If an external source causes an increase of the energy of the sensing element $\mathrm{d}Q$, the optical signal will be determined as

$$\Phi=\frac{\mathrm{d}Q}{\mathrm{d}t}=T\frac{\mathrm{d}S}{\mathrm{d}t}. \tag{54}$$

If we assume that the temperature variation ΔT is the generalized force and the rate of entropy change $\dot{S}$ is the generalized velocity, we obtain the generalized impedance for the harmonic excitation ($\varepsilon_1=1$)

$$Z(\omega)=\frac{\Delta T}{\dot{S}}=\frac{T}{G_{\text{th}}+j\omega C_{\text{th}}}. \tag{55}$$

Introducing a thermal time constant $\tau_{\text{th}}=C_{\text{th}}R_{\text{th}}$, the real part of the thermal impedance becomes

$$R_{\text{th}}(\omega)=\frac{T}{G_{\text{th}}(1+\omega^2\tau_{\text{th}}^2)}. \tag{56}$$

Using Eq. (12), it is easy to obtain that the spectral density of thermal fluctuations is

$$\overline{\Delta T^2}=(4kT^2R_{\text{th}})/(1+\omega^2\tau_{\text{th}}^2). \tag{57}$$

Thus, it follows that in this case, the mean square fluctuation of the optical power caused by the background radiation and emitted by the active area of the detector is given as

$$\overline{\Delta P^2}=4kT^2G_{\text{th}}. \tag{58}$$

This expression is valid if the detector temperature T_{d} and the background temperature T_{b} are equal. In the case when these two temperatures are different, the fluctuation–dissipation theorem cannot be utilized to determine $\overline{\Delta P^2}$, as mentioned in Section 1. The calculation of $\overline{\Delta P^2}$ is considered in detail in our article [8], and enclosed here is only the final result.

Assuming that the active area of the thermal detector is A and its emissivity 1, and if the radiation field corresponds to a temperature T, for a field of view θ, the mean square fluctuation of the incident power is

$$\overline{\Delta P^2}=8\sin^2(\theta/2)A\sigma kT^5\Delta f, \tag{59}$$

where Δf denotes the bandwidth. For $\theta=180^\circ$ and assuming different temperatures of the detector and the background we obtain

$$\overline{\Delta P^2}=8A\sigma k(T_{\text{b}}^5+T_{\text{d}}^5)\Delta f. \tag{60}$$

In the case of the membrane structures for thermal detectors, it is convenient to divide the total thermal conductance G_{th} into three independent parts: G_{leg}, G_{gas}, G_{rad}.

G_{leg} is the heat conductance through the legs supporting the membrane, G_{gas} the corresponding conductance through the surrounding gas, and the third component is due to thermal radiation.

In the situations where the environment temperature is approximately equal to the temperature of the sensing element, we can introduce radiation thermal conductance. Starting from the fact that the total radiation losses are

$$P=\varepsilon_{\text{eff}}\sigma A_{\text{memb}}T^4, \tag{61}$$

we obtain the expression for G_{rad}:

$$G_{\text{rad}}=\mathrm{d}P/\mathrm{d}t=4\varepsilon_{\text{eff}}\sigma A_{\text{memb}}T^3, \tag{62}$$

where ε_{eff} is the effective emissivity, A_{memb}, the area of the membrane surface and T, the absolute temperature.

To calculate G_{leg}, the membrane geometry and the thermal conductivity λ of the material must be known. Usually, we assume that the contribution to G_{leg} is completely due to the conduction through the supporting leg, and the conduction within the membrane is negligible.

The thermal conductance G_{leg} of the membrane supported by two legs is

$$G_{\text{leg}}=2\lambda_{\text{leg}}\frac{A_{\text{leg}}}{l_{\text{leg}}}. \tag{63}$$

A_{leg} is the cross-sectional area and l_{leg} is the average length of the legs, respectively.

G_{gas} can be divided into two parts, due to heat conduction G_{cond} and the heat transfer due to convection G_{conv} through the surrounding gas. Usually, $G_{\text{gas}}\approx G_{\text{cond}}$, $G_{\text{conv}}\ll G_{\text{cond}}$. Due to this

$$G_{\text{cond}}=\lambda_{\text{gas}}A_{\text{memb}}/d, \tag{64}$$

where d is the membrane to substrate spacing. λ_{gas}, thermal conductivity of the gas, exhibits a strong dependence on the ambient pressure p.

A simple consideration shows that [22]

$$1/\lambda_{\text{gas}} = 1/\lambda_{\text{hp}} + (1/\gamma_{\text{lp}}d)(1/p). \tag{65}$$

λ_{hp} is a pressure-independent thermal conductivity dominating in the high-pressure regime, γ_{lp} is the thermal conductivity for unit pressure and length which dominates in the low-pressure regime.

Further, we obtain

$$1/G_{\text{cond}} = (1/\lambda_{\text{hp}})(d/A_{\text{memb}}) + (1/\gamma_{\text{lp}})(1/p)(1/A_{\text{memb}}), \tag{66}$$

and for the air as the gas ambience [22] $\lambda_{\text{hp}} = 0.026$ W/km, $\gamma_{\text{lp}} = 1.9$ m/s K.

As an illustration, we present in Fig. 4, the dependence of the thermal conductance on gas pressure for two different membranes, where the area of the larger membrane is $A_{\text{memb 1}} = 100 \times 100$ μm^2, and the area of the other membrane $A_{\text{memb 2}} = 50 \times 50$ μm^2 [22]. The solid line represents the results of the calculation using the above approach, where nitrogen was used as the model for air. The detector structure is shown in the inset.

It is clear from Fig. 4 that G_{th} reaches a constant value if the pressure is decreased below 0.01 mbar, when G_{leg} starts to dominate in G_{th}. Besides this, G reaches a practically constant value at the atmospheric pressure, when the contribution of G_{gas} to the thermal conductance is greatest.

We conclude that basically there are three possible cases: (1) the membrane is surrounded by air at atmospheric pressure; (2) the membrane is in vacuum; (3) the heat dissipation from the membrane is dominated by radiation losses. The order of magnitude for the above three cases is $G_{\text{th}} = (2.0 \times 10^{-5},\ 2.3 \times 10^{-7},\ 7.0 \times 10^{-9})$ W/K, respectively, whereas $A_{\text{memb}} = 50 \times 50$ μm^2.

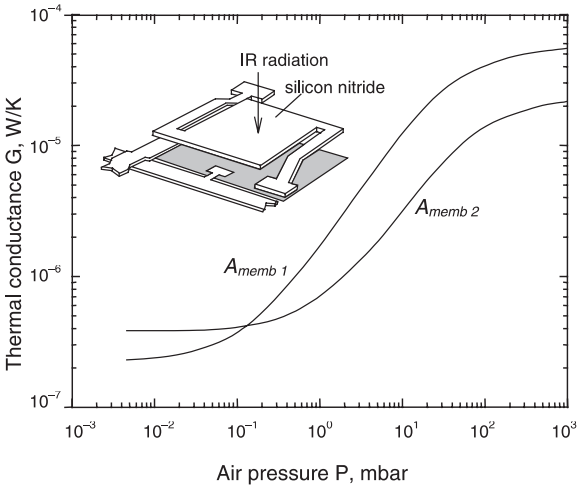

Fig. 4. Dependence of the thermal conductance on gas pressure for two membranes, $A_{\text{memb 1}} = 100 \times 100$ μm^2, $A_{\text{memb 2}} = 50 \times 50$ μm^2. Detector structure is shown in the inset.

The heat capacity or thermal mass of the membrane C is given as

$$C = V\rho c\ (J/K), \tag{67}$$

where V is the detector volume, ρ is the density and c is the specific heat. For a silicon nitride (Si_3N_4) membrane, the thermal time constant for the three above cases is (77 μs, 6.7 ms, 0.2 s).

4. Examples

The operation of vibrational MEMS devices (sensors, actuators, electronic and mechanical parts, oscillators, filters) can be divided into two groups. One of these groups, for instance pressure sensors and thermal IR detectors, most often operate at frequencies much below the resonant frequency. The other group, including resonant gyroscopes and micromechanical oscillators, etc. operate at frequencies near the resonant frequency.

It is easy to show that the displacement noise X_n^2 peaks at the resonant frequency (at which e.g. oscillators and micromechanical filters operate). Note that this noise is Q times larger than that for the mechanical devices operating below resonance (e.g. capacitive accelerometers). Namely, let us remember that

$$X_n^2(\omega) = \frac{4kT}{\omega_0 Q\kappa} G^2(\omega). \tag{68}$$

For a resonant frequency $\omega = \omega_0$, we have

$$X_n^2 = \frac{4Q\sqrt{m}}{\kappa^{3/2}} kT. \tag{69}$$

If $\omega \ll \omega_0$

$$X_n^2 = \frac{4\sqrt{m}}{Q\kappa^{3/2}} kT. \tag{70}$$

Besides numerous parameters characterizing the MEMS parts, we are mostly interested in those connected with the noise in these structures. One such parameter is the minimum detectable signal (MDS). The MDS of a system is typically defined to be equal to the rms, equivalent input noise. For example, in the case of the pressure sensors, the MDS is expressed as an equivalent pressure fluctuation

$$P_n = \sqrt{4kTR_{\text{acs}}\,\Delta f} = \sqrt{\frac{4kT\omega_0 m\kappa\,\Delta f}{S^2 Q\kappa}} = \sqrt{\frac{4\kappa kT\,\Delta f}{S^2\omega_0 Q}}, \tag{71}$$

where R_{acs} is acoustic resistance, $R_{\text{acs}} = R/S^2$ and S is the area of the active face.

4.1. Accelerometer

An accelerometer is an inertial sensor used to measure acceleration. Between many MEMS-based accelerometers we consider the capacitive sensing scheme for acceleration detection [23]. A simplified schematic capacitive accelerometer is shown in Fig. 5.

The minimum detectable acceleration is determined by the total noise referred back to accelerometer input. We consider two noise sources: one is the thermal–mechanical noise and, the second is the transistor noise in the front-end circuit.

To obtain noise on the input, it is necessary to find the accelerometer sensitivity. This sensitivity is defined as the ratio of the output voltage and the input acceleration. It is defined by both the mechanical sensitivity and the position sense circuit. The mechanical sensitivity is defined as how much the proof mass moves when an acceleration is applied

$$\frac{x}{a} = \frac{m}{-m\omega^2 + j\omega R + \kappa} = \frac{1}{-\omega^2 + j\omega\omega_r/Q + \omega_r^2}, \tag{72}$$

where $\omega_r = (\kappa/m)^{1/2}$ and $Q = \omega_r m/R$. At frequencies well below resonance ($\omega \ll \omega_r$), the mechanical sensitivity is

$$x/a = 1/\omega_r^2 = m/\kappa. \tag{73}$$

From this equation, we can see that the mechanical sensitivity is inversely proportional to the square of the resonant frequency.

Usually, we choose a commonly used single-ended half bridge capacitive sense interface to translate the proof mass displacement into the output voltage, as shown in Fig. 5.

In Fig. 6, C_1 and C_2 are capacitors between the movable finger and its nearest fixed finger. The modulation voltage V_m is applied between fingers. C_{para} is the total parasitic capacitance at the output.

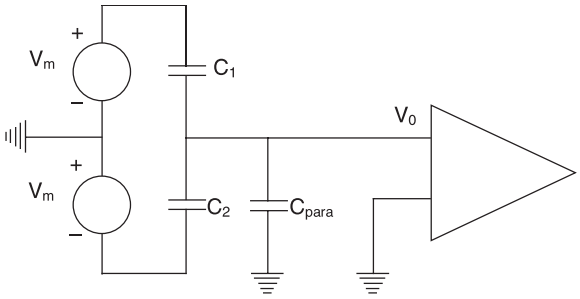

Fig. 6. Accelerometer sensing interface.

Simple analysis gives

$$V_0 = \frac{C_1 - C_2}{C_1 + C_2 + C_{\text{para}}} V_{\text{m}}. \tag{74}$$

If no acceleration occurs, the movable fingers are midway between two fixed sense fingers (inset in Fig. 4), $C_1 = C_2 = C_0$ and $V_0 = 0$.

Under an applied acceleration, the proof mass moves and C_1 and C_2 are no longer equal. Using Fig. 5 and assuming that the displacement x is small compared to the initial gap g_0:

$$C_1 - C_2 = 2C_0 x/g_0. \tag{75}$$

Combining Eqs. (73)–(75), we obtain the sensitivity as

$$\frac{V_0}{a} = \frac{2C_0}{2C_0 + C_{\text{para}}} \frac{m}{\kappa g_0} V_{\text{m}}. \tag{76}$$

According to Eqs. (18) and (74), the noise equivalent acceleration is obtained as

$$a_n = \omega_r^2 X(\omega) = \omega_r^2 \sqrt{\frac{4kT}{\omega_r Q \kappa}}. \tag{77}$$

The noise voltage at the input due to the thermal–mechanical noise is given as

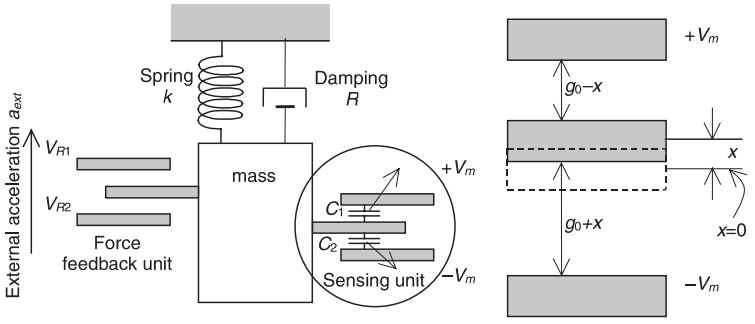

Fig. 5. Schematic representation of a capacitive accelerometer.

$$V_n = \sqrt{\frac{4kT}{\omega_r Q \kappa}} \frac{1}{g_0} \frac{2C_0}{2C_0 + C_{\text{para}}} V_{\text{m}} \Delta f. \tag{78}$$

Let $V_{\text{n-circuit}}$ be the noise arriving from the electrical circuit. If we direct this noise into the input acceleration we obtain

$$a_{\text{n-circuit}} = V_{\text{n-circuit}}/\text{sensitivity}. \tag{79}$$

The minimum detectable acceleration to the total input acceleration noise

$$a_{\text{nt}} = \sqrt{a_{\text{n-circuit}}^2 + a_n^2}, \tag{80}$$

and the total noise voltage is

$$V_{\text{nt}} = \sqrt{V_n^2 + V_{\text{n-circuit}}^2}. \tag{81}$$

4.2. Scanning probe microscope

Scanning probe microscopes with micromechanical cantilevers are commonly used for detection of small forces. A fundamental limit to the measurement of small forces is imposed by thermomechanical noise, which is governed by dissipation of mechanical energy in the force-measuring cantilever.

Thus, the minimum detectable force is equal to the noise force which according to Eq. (12) can be written as

$$F_{\text{min}} = \sqrt{4kTR(\omega)\,\Delta f}, \tag{82}$$

or, if expressed by the microcantilever Q-factor and its resonant frequency ω_0:

$$F_{\text{min}} = \sqrt{\frac{4kT\kappa\,\Delta f}{\omega_0 Q}}. \tag{83}$$

This minimum detectable force can also be expressed in terms of the cantilever dimensions; w is the cantilever width, l is the cantilever length, and t is the cantilever thickness. Let us consider only the first oscillatory mode for which the following is valid:

$$\omega_0 = \frac{(1.875)^2}{l^2}\sqrt{\frac{EI}{m}}, \quad \kappa = \frac{3EI}{l^4}, \quad I = \frac{wt^3}{12}. \tag{84}$$

It should be borne in mind that in the expression for the resonant frequency m is given per unit length. After the replacement into Eq. (83), we obtain [24]:

$$F_{\text{min}} = \left(\frac{wt^2}{lQ}\right)^{1/2} (E\rho)^{1/4} (kT\,\Delta f)^{1/2}, \tag{85}$$

where E is the elasticity modulus, and ρ is the mass density of the cantilever material.

It can be concluded from Eq. (85) that an ultrasensitive cantilever can be obtained if narrow, thin and long cantilever is used. It is true only if a high mechanical Q-factor is provided.

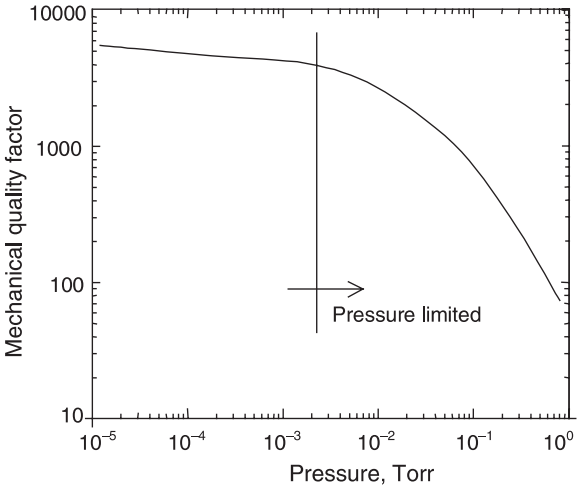

Fig. 7. Dependence on the mechanical Q factor on pressure for a silicon nitride cantilever [25].

One of the important dissipation sources in micromechanical oscillators is air damping. Fig. 7 shows the dependence of the Q-factor on the air pressure for a silicon nitride cantilever of a 5100 Å thickness.

It is interesting to note that the investigations showed that the Q-factor measured in high vacuum (10^{-6} Torr):

- does not depend on the cantilever length;
- does not depend on the cantilever width;
- becomes linearly higher with an increase in the cantilever thickness.

This shows that the dissipation is not caused by internal losses in bulk but rather by surface losses. The possible sources of the surface losses are adsorbates on the cantilever surface or surface defects created during fabrication. A confirmation to this is the fact that, in some cases, Q can be dramatically increased by annealing in the forming gas (Ar with 4.25% H_2) for 1 h at a temperature of 700°C.

The results of these investigations show that extremely good results with an ultra-high sensitivity cantilevers can be obtained by the special surface treatment.

Let us finally quote a result obtained by the use of Si single-crystalline cantilever that is 600 Å thick, 220 μm long and about 5 μm wide, with a resonant frequency at $f_0 = 1.7$ kHz, $Q = 6700$ and $\kappa = 6.5 \times 10^{-6}$ N/m for a force noise spectral density as given in Ref. [3]:

$$F_{\text{min}} = 5.68 \times 10^{-18}\ \text{N/Hz}^{1/2}.$$

Another example is the piezoresistive atomic force microscope (AFM) cantilevers. Ref. [25] presents a piezoresistive cantilever with a length $l \approx 10$ μm, width about 2 μm and thickness 0.35 μm. The displacement

sensitivity $(\Delta R/R)/\mathring{A} = 1.1 \times 10^{-5}$, the displacement resolution 2×10^{-3} $\mathring{A}/Hz^{1/2}$, the mechanical response time is less than 90 ns, and the stiffness is 2 N/m. This microcantilever has been fabricated from a silicon-on-insulator wafer. A shallow boron implant ($6 \times 10^{13}/cm^2$, 10 keV) is used to form piezoresistors at the base of the cantilever. The piezoresistors are confined to the base of the cantilever because this is the region where the largest stresses are induced in response to the tip deflection.

Let us determine the sensitivity first. We start from

$$\Delta R/R = \sigma_{max}\pi_{eff}, \tag{86}$$

where ΔR is the piezoresistor resistance change, π_{eff}, the effective piezoresistive coefficient and σ_{max}, the maximum mechanical stress of the cantilever. The deflection of a cantilever with a length l, width w and thickness t is

$$y(x) = F(x^2 l - x^3/3)/2EI, \tag{87}$$

where F is the applied force at the free end of the microcantilever. The stress at the upper surface $\sigma(x)$ is

$$\sigma(x) = 6F(l - x)/t^2 w, \tag{88}$$

so that

$$\sigma_{max} = 6FL/t^2 w. \tag{89}$$

The maximum deflection can be determined using the force F as

$$y_{max} = \frac{4Fl^3}{Ewt^3}, \quad \therefore F = \frac{y_{max} Ewt^3}{4l^3}, \tag{90}$$

thus,

$$\sigma_{max} = \frac{3}{2}\frac{Et}{l^2} y_{max}. \tag{91}$$

On the contrary, the resonant frequency of this cantilever can be expressed as

$$f_0 = 0.16(E/\rho)^{1/2}(t/l^2); \tag{92}$$

hence,

$$\sigma_{max} = (3/0.32) f_0 (\rho E)^{1/2} y_{max}, \tag{93}$$

Therefore,

$$\Delta R/R = 0.94 f_0 (\rho E)^{1/2} \pi_{eff} y_{max}. \tag{94}$$

In the previous text, we saw that the displacement noise spectral density of a cantilever at the resonant frequency f_0 is given as

$$|y_{max}|_n = \frac{1}{2\pi f_0}\sqrt{\frac{4kT}{R_m}}, \tag{95}$$

where R_m is mechanical resistance. Using Eq. (94), we obtain

$$\left|\frac{\Delta R}{R}\right|_n = 1.5\sqrt{\rho E}\,\pi_{eff}\sqrt{\frac{4kT}{R_m}}. \tag{96}$$

The authors of Ref. [25] report that their cantilevers have a sufficient displacement resolution to detect their own mechanical–thermal noise in vacuum and, for some designs, even in air. In one of their experiments, they obtained that the thermal–mechanical noise appeared as a distinct peak with a quality factor of 30 at 1.1 MHz resonant frequency of the cantilever. The explanation is connected with Eqs. (77) and (78) wherein it can be seen that the decrease of the cantilever dimensions according to Eq. (46) causes a decrease of the mechanical resistance so that the thermal mechanical noise becomes more pronounced.

4.3. Infrared thermal detectors

In the course of the past year, a number of infrared room-temperature thermal detectors were fabricated by the micromachining processes which were 100% compatible with the silicon integrated circuits processing [5,8,26–28]. These parameters are expected to approach the theoretical values because their sensitivity is high and the noise is low. Most of these MEMS detectors base their operation on the deflection measurement.

In our previous work [8], we analyzed a new type of pneumatic detector utilizing thermal expansion of gas to detect IR radiation. To detect this gas expansion, a tunneling deflection sensor is used. We showed that a good agreement with experimental noise equivalent power (NEP) is obtained only if the thermal–mechanical noise is taken into account.

Here we consider the case of an IR detector based on the bimaterial concept (Fig. 8).

The bimaterial element comprises two coupled cantilevers with different expansion coefficients α_1 and α_2. Temperature changes cause the deflection of the cantilever. The deflection depends on the ratio of the cantilever thicknesses $n = t_2/t_1$ and on the ratio of their Young's moduli, $\Phi = E_1/E_2$.

The calculations show that the deflection dependence on the temperature is [29,30]

$$\delta(T) = \frac{3L^2}{8t_1}(\alpha_1 - \alpha_2)\frac{8(1+n)(T - T_0)}{4 + 6n + 4n^2 + n^3\Phi + 1/n\Phi}, \tag{97}$$

where T_0 is the temperature at which the deflection equals zero.

Let us remind ourselves that the active area temperature increase for all kinds of thermal detectors is in the first approximation [5]

$$\Delta T = R_{th} P\left(1 + \omega^2 \tau_{th}^2\right)^{-1/2}, \tag{98}$$

where P is the absorbed optical power, whereas the other parameters are previously defined.

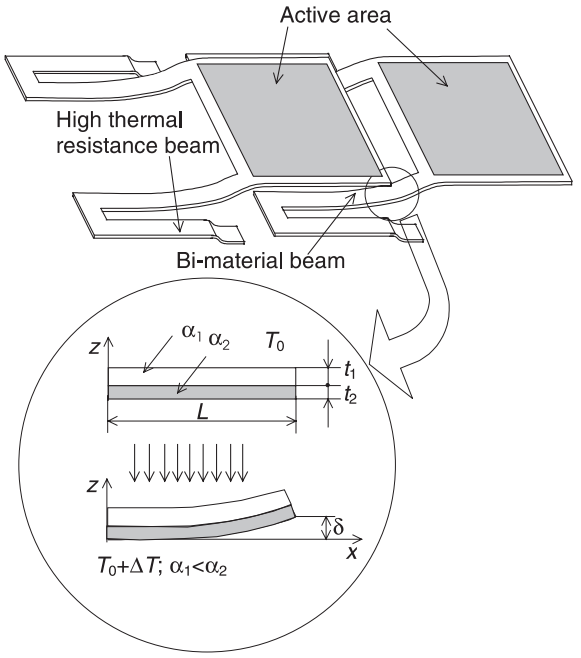

Fig. 8. The IR detector based on the bimaterial concept.

In the case of bimaterial detectors, the measured value is the displacement of the active area due to the temperature change (Fig. 8). To this purpose, we define the sensitivity of the bimaterial effect as

$$\beta = \Delta\delta/\Delta T = K\Delta\alpha L^2/t_1 \tag{99}$$

so that the displacement due to the temperature change is given as

$$\Delta\delta = \beta R_{\text{th}} P/(1+\omega^2\tau_{\text{th}}^2)^{1/2}. \tag{100}$$

In the case of bimaterial detectors, there are two basic mechanisms of noise generation due to the temperature fluctuations: The first one causes the spectral density of thermal fluctuations

$$\overline{\Delta T^2} = \frac{4kT^2 R_{\text{th}}}{1+\omega^2\tau_{\text{th}}^2}. \tag{101}$$

The other one is the thermal mechanical noise, where the displacement spectral density is given as

$$\overline{\Delta\delta^2} = \frac{4kT}{\omega\kappa Q} G^2(\omega). \tag{102}$$

The noise equivalent displacement is

$$NE\,\delta^2 = \beta^2\,\overline{\Delta T^2} + \overline{\Delta\delta^2} \tag{103}$$

so that the detectivity of a thermal bimaterial detector with a 2π field of view

$$D^* = \frac{\sqrt{A}}{\sqrt{\frac{4kT^2}{R_{\text{th}}} + \frac{4kT}{\omega_0\kappa Q}\frac{1}{\beta^2}\frac{1}{R_{\text{th}}^2}\left(1+\omega^2\tau_{\text{th}}^2\right)G^2(\omega)}}. \tag{104}$$

The above expression shows that the specific detectivity D^* depends both on thermal and mechanical properties of the detector. As both the thermal resistance and the Q factor increase with a pressure decrease around the sensing element, it follows that in principle a convenient choice of other parameters (bimaterial sensitivity β and stiffness κ) a detectivity can be reached which is approximately equal to the background limited value ($D^* = 1.81 \times 10^{10}$ cm Hz$^{1/2}$/W).

So our calculations [31] show that for a bimaterial detector with the active area dimensions $\sim 75 \times 75$ μm^2, thermal conductivity $G_{\text{th}} = 1.76 \times 10^{-7}$ W/K, $\tau_{\text{th}} = 22.7$ ms and with the mechanical parameters $\kappa = 0.02$ N/m, resonant frequency $f_0 = 6.3$ kHz, $Q = 1000$ and bimaterial sensitivity $\beta = 0.14 \times 10^{-6}$ m/K at a frequency of 15 Hz, we obtain $D^* = 7 \times 10^9$ cm Hz$^{1/2}$/W, which is within a factor 2 with regard to the background detectivity. At the same time, the ratio of the thermal and mechanical part of the term under the square root is ≈4.

5. Conclusion

The importance of noise investigation in an MEMS is contained in the connection of the MDS (minimum detectable signal) with its geometrical and physical parameters, with the aim to optimize the design.

In this work, we mostly considered noises caused by the temperature fluctuations. In the case of mechanical systems, it is the thermal–mechanical noise, and in the system where heat conduction appears, it is the thermal noise (sometimes referred to as phonon noise).

All kinds of noises are connected with dissipative processes. In the case of mechanical systems, they are characterized by the real part of the mechanical impedance (or admittance), and in the case of thermal processes, most often by the thermal conductance.

The work discusses only the most often encountered dissipative processes, those caused by the viscosity of the medium. However, there are a number of various internal dissipative processes, the mechanism of which is still not clear enough. As an example, we quote the dissipative processes in the supports of various kinds of cantilevers, etc.

It should be mentioned that there are noises caused by the processes of adsorption and desorption of molecules and leading to the stochastic changes of the mass of miniature active parts of the MEMS. It is not simple to include these into the dissipative processes.

Thus, as the final conclusion, it may be said that the investigation of noises in the MEMS is currently in its infancy and the field of application of MEMS is very

broad (physics, chemistry, biology, medicine), the mechanisms determining the ultimate performance of the MEMS are very diverse and should be well studied.

References

[1] Elwenspoek M. Etching technology. UETP-MEMS, FSRM, 1995.

[2] Nguyen CTC. Microelectromechanical components for miniaturized low-power communications. In: Proc 1999 IEEE-MTT-s Int Microwave Symp RF MEMS Workshop. Annaheim, California, 1999. p. 48–77.

[3] Stowe TD, Yasamura K, Kenny TW, Botkin D, Wago K, Rugar D. Atonewton force detection using ultrathin silicon cantilevers. Appl Phys Lett 1997;71:288–90.

[4] Nguyen CTC. Frequency-selective MEMS for miniaturized communication devices. In: Proc 1998 Aerospace Conf vol 1, Snowman, Colorado, 1998. p. 445–60.

[5] Djurić Z. New generation of thermal infrared detectors. In: Proc 20th Int Conf Microelectro MIEL 95. vol. 2, Niš, Serbia, 1995. p. 559–64.

[6] Bordoni F, D'Amico A. Noise in sensors. Sensors and Actuators A 1990;A21–A23:17–24.

[7] Gabrielson TB. Mechanical–thermal noise in micromachined acoustic and vibration sensors. IEEE Trans Electron Dev 1993;40:903–9.

[8] Djurić Z, Matović J, Randjelović D, Jakšić Z, Danković T. Noise in micromechanical structures caused by temperature fluctuations. In: Proc Fifth Workshop on Thermal Aspects in Microsystem Technology NEXUSPAN, Budapest, Hungary, 1998. p. 142–51.

[9] Braginskiy VB, Manukin AB. Izmereniye Mal'ih sil v fixicheskih eksperimentah. Nauka, Moscow, 1974.

[10] Saulson PR. Thermal noise in mechanical experiments. Phys Rev D 1990;42:2437–45.

[11] Huang YL, Saulson PR. Dissipation mechanisms in pendulums and their implication for gravitational wave interferometers. Rev Sci Instrum 1998;69:544–53.

[12] Yong YK, Vig JR. Resonator surface contamination – a. cause of frequency fluctuations. IEEE Trans Ultrason Ferroelectrics Freq Contr 1989;36:4.

[13] Nguyen CTC. Micromechanical resonators for oscillators and filters. In: Proc 1995 IEEE Int Ultra-sonics Symp Seattle, WA, 1995. p. 489–99.

[14] Landau LD, Lifshitz EM. Statisticheskaya Fizika. vol. 1, Mir, Moscow, 1976.

[15] Landau LD, Lifshitz EM. Teoriya uprugosti. vol. 1, Mir, Moscow, 1975.

[16] Gillespie D. Thermal noise in the initial LIGO interferometers. Ph.D. Thesis, California Institute of Technology, Pasadena, CA, 1995.

[17] Callen HB, Welton TA. Irreversibility and generalized noise. Phys Rev 1951;83:34–40.

[18] Salapaka MV, Bergh HS, Lai J, Majumdar A, McFarland E. Multi-mode noise analysis of cantilevers for scanning probe microscopy. J Appl Phys 1997;81:2480–5.

[19] Tilmans HA. Equivalent circuit representation of electromechanical transducers: II distributed-parameters systems. J Micromech Microengng 1997;7:285–309.

[20] Strelkov P. Vvedeniye v teoriyu kolebaniy. Mir, Moscow, 1964.

[21] Vejola T, Kuisma H, Lahdenpero J. The influence of gas-surface interaction on gas film damping in a silicon accelerometer. Sensors and Actuators A 1998;A66:83–92.

[22] Eriksson P, Andersson JA, Stemme G. Thermal characterization of surface-micromachined silicon nitride membranes for thermal infrared detectors. IEEE J Microelectromech Syst 1997;6:55–61.

[23] Zhou Y. Layout Synthesis of Accelerometers. Carnegie Melon University, 1998.

[24] Yasumura KY, Stowe TD, Chow EM, Pfafman T, Kenny TW, Rugar D. A study of microcantilever quality factor. J Microelectromech Syst, submitted for publication.

[25] Read RP, Mamin HJ, Terris BD, Fan LS, Rugar D. 6-MHz 2-N/m piezoresistive atomic-force-microscope cantilevers with INCISIVE tips. IEEE J Microelectromech Syst 1997;6:294–302.

[26] Wood RA. Uncooled thermal imaging with monolythic silicon focal plane. Proc SPIE 1993;2020:322–9.

[27] Chevrier JB, Baert K, Slater T. An infrared pneumatic detector made by micromachining technology. J Micromech Microengng 1995;5:193–5.

[28] Kenny TW, Kaiser W, Waltman SB, Reynolds JK. Novel infrared detector based on a tunneling displacement transducer. Appl Phys Lett 1991;59:1820–2.

[29] Lai J, Perazzo T, Shi Z, Majumdar A. Optimization and performance of micro-optomechanical thermal sensors. Sensors and Actuators A 1997;A58:113–9.

[30] Amantec R, Knoedler CM, Pantuso FP, Patel VK, Saues DJ, Tower JR. An uncooled IR imager with 5 mK NEDT. Proc SPIE 1997;3061:210–22.

[31] Matović J, Djurić Z. Infrared detector for direct conversion of IR radiation to visible scene. submitted for publication.